

Loss Landscapes of Regularized Linear Autoencoders

Daniel Kunin^{* 1} Jonathan M. Bloom^{* 2} Aleksandrina Goeva² Cotton Seed²

Abstract

Autoencoders are a deep learning model for representation learning. When trained to minimize the Euclidean distance between the data and its reconstruction, linear autoencoders (LAEs) learn the subspace spanned by the top principal directions but cannot learn the principal directions themselves. In this paper, we prove that L_2 -regularized LAEs learn the principal directions as the left singular vectors of the decoder, providing an extremely simple and scalable algorithm for rank- k SVD. More generally, we consider LAEs with (i) no regularization, (ii) regularization of the composition of the encoder and decoder, and (iii) regularization of the encoder and decoder separately. We relate the minimum of (iii) to the MAP estimate of probabilistic PCA and show that for all critical points the encoder and decoder are transposes. Building on topological intuition, we smoothly parameterize the critical manifolds for all three losses via a novel unified framework and illustrate these results empirically. Overall, this work clarifies the relationship between autoencoders and Bayesian models and between regularization and orthogonality.

1. Introduction

Consider a data set consisting of points x_1, \dots, x_n in \mathbb{R}^m . Let $X \in \mathbb{R}^{m \times n}$ be the data matrix with the columns x_i . We will assume throughout that $k \leq \min\{m, n\}$ and that the singular values of X are positive and distinct.

An *autoencoder* consists of an encoder $f : \mathbb{R}^m \rightarrow \mathbb{R}^k$ and decoder $g : \mathbb{R}^k \rightarrow \mathbb{R}^m$; the latter maps the latent representation $f(x_i)$ to the reconstruction $\hat{x}_i = g(f(x_i))$ (Goodfellow et al., 2016). The full network is trained to minimize reconstruction error, typically the squared Euclidean distance between the dataset X and its reconstruction \hat{X} (or equivalently, the Frobenius norm of $X - \hat{X}$). When the activations

of the network are the identity, the model class reduces to that of one encoder layer $W_1 \in \mathbb{R}^{k \times m}$ and one decoder layer $W_2 \in \mathbb{R}^{m \times k}$. We refer to this model as a *linear autoencoder* (LAE) with loss function defined by

$$\mathcal{L}(W_1, W_2) = \|X - W_2 W_1 X\|_F^2.$$

Parameterizing \mathcal{L} by the product $W = W_2 W_1$, the Eckart-Young Theorem (Eckart & Young, 1936) states that the optimal W orthogonally projects X onto the subspace spanned by its top k principal directions¹.

Without regularization, LAEs learn this subspace but cannot learn the principal directions themselves due to the symmetry of \mathcal{L} under the action of the group $\text{GL}_k(\mathbb{R})$ of invertible $k \times k$ matrices defined by $(W_1, W_2) \mapsto (GW_1, W_2 G^{-1})$:

$$X - (W_2 G^{-1})(GW_1)X = X - W_2 W_1 X. \quad (1)$$

Indeed, \mathcal{L} achieves its minimum value on a smooth submanifold of $\mathbb{R}^{k \times m} \times \mathbb{R}^{m \times k}$ diffeomorphic to $\text{GL}_k(\mathbb{R})$; the learned latent representation is only defined up to deformation by invertible linear maps; and the k -dimensional eigenspace of W with eigenvalue 1 has no preferred basis.

In light of the above, the genesis of this work was our surprise at the empirical observation in Plaut (2018) that the principal directions of X are recovered from a trained LAE as the left singular vectors of the decoder (or as the right singular vectors of the encoder). While the paper made no mention of it, we realized by looking at the code that training was done with the common practice of L_2 -regularization:

$$\mathcal{L}_\sigma(W_1, W_2) = \mathcal{L}(W_1, W_2) + \lambda (\|W_1\|_F^2 + \|W_2\|_F^2).$$

In this paper, we prove that LAEs with L_2 -regularization do in fact learn the principal directions in this way. We further show how to recover those eigenvalues larger than the regularization constant λ .

¹The principal directions of X are the eigenvectors of the covariance of X in descending order by eigenvalue, or equivalently the left singular vectors of the mean-centered X in descending order by (squared) singular values.

^{*}Equal contribution ¹Institute for Computational and Mathematical Engineering, Stanford University, Stanford, California, USA ²Broad Institute of MIT and Harvard, Cambridge, Massachusetts, USA.

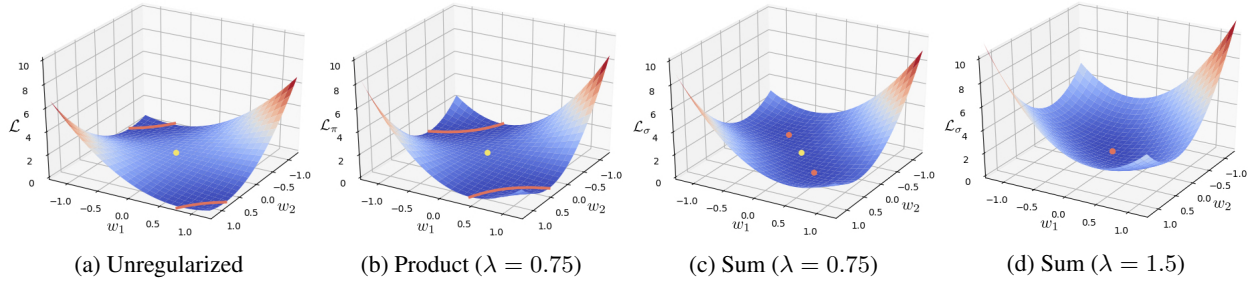


Figure 1. Loss landscapes with $n = m = k = x = 1$. Yellow points are saddles and red curves and points are global minima.

1.1. Related work

Building on the original work of [Eckart & Young \(1936\)](#) on low-rank matrix approximation, [Izenman \(1975\)](#) demonstrated a connection between a rank-reduced regression model similar to an LAE and PCA. [Boulevard & Kamp \(1988\)](#) characterized the minima of an unregularized LAE; [Baldi & Hornik \(1989\)](#) extended this analysis to all critical points.

Several studies of the effect of regularization on LAEs have emerged of late. The rank-reduced regression model was extended in [Mukherjee & Zhu \(2011\)](#) to the study of rank-reduced ridge regression. A similar extension of the LAE model was given in [Josse & Wager \(2016\)](#). An in depth analysis of the linear denoising autoencoder was given in [Pretorius et al. \(2018\)](#) and most recently, [Mianjy et al. \(2018\)](#) explored the effect of dropout regularization on the minima of an LAE.

While L_2 -regularization is a foundational technique in statistical learning, its effect on autoencoder models has not been fully characterized. Recent work of [Mehta et al. \(2018\)](#) on L_2 -regularized deep linear networks applies techniques from algebraic geometry to highlight how algebraic symmetries result in “flat” critical manifolds and how L_2 -regularization breaks these symmetries to produce isolated critical points. We instead apply (deeply connected) techniques from algebraic topology to completely resolve dynamics in the special case of LAEs.

1.2. Our contributions

The contributions of our paper are as follows.

- In Section 2 we consider LAEs with (i) no regularization, (ii) regularization of the composition of the encoder and decoder, and (iii) regularization of the encoder and decoder separately as in \mathcal{L}_σ . We build intuition by analyzing the scalar case, relate the losses to denoising and contrastive LAEs, reflect on the relationship between regularization and orthogonality, and deduce that the encoder and decoder are transposes for all critical points of \mathcal{L}_σ .
- In Section 3, we realize all three LAE models as gener-

ative processes, most notably relating the minimum of \mathcal{L}_σ and the MAP estimate of probabilistic PCA.

- In Section 4, we embark on the technical work of characterizing all three loss landscapes. To build intuition, we first leave the overparameterized world of coordinate representations to think deeply about the squared distance from a plane to a point cloud. We expand on this topological viewpoint in Appendix B.
- In Section 5, we illustrate these results empirically, with all code available².
- In Section 6, we discuss this work and potential next steps.

The connections we draw between regularization and orthogonality, LAEs and probabilistic PCA ([Tipping & Bishop, 1999](#)), and the topology of Grassmannians are novel and provide a deeper understanding of the loss landscapes of regularized linear autoencoders.

2. Regularized LAEs

In the appendix (A), we provide a self-contained derivation of the fact that an LAE with bias parameters is equivalent to an LAE without bias parameters trained on mean-centered data ([Boulevard & Kamp, 1988](#)). So without loss of generality, we will assume X is mean centered and consider the following three LAE loss functions:

$$\mathcal{L}(W_1, W_2) = \|X - W_2 W_1 X\|_F^2$$

$$\mathcal{L}_\pi(W_1, W_2) = \mathcal{L}(W_1, W_2) + \lambda \|W_2 W_1\|_F^2$$

$$\mathcal{L}_\sigma(W_1, W_2) = \mathcal{L}(W_1, W_2) + \lambda (\|W_1\|_F^2 + \|W_2\|_F^2)$$

We call these the **unregularized**, **product**, and **sum** losses, respectively.

2.1. Visualizing LAE loss landscapes

We can visualize these loss functions directly in the case $n = m = k = 1$, as shown in Figure 1. In fact, working out the critical points in this scalar case led us to conjecture the general result in Section 4. We invite the reader to enjoy

²github.com/danielkunikin/Regularized-Linear-Autoencoders

deriving the following results for themselves.

For all three losses, the origin $w_1 = w_2 = 0$ is the unique rank-0 critical point. For \mathcal{L} and \mathcal{L}_π , the origin is always a saddle point, while for \mathcal{L}_σ the origin is either a saddle point or global minimum depending of the value of λ .

For \mathcal{L} , the global minima are rank-1 and consist of the hyperbola³

$$w_2 w_1 = 1.$$

For \mathcal{L}_π , the global minima are rank-1 and consist of this hyperbola shrunk toward the origin as in ridge regression,

$$w_2 w_1 = (1 + \lambda x^{-2})^{-1}.$$

For \mathcal{L}_σ the critical points depend on the scale of λ relative to x^2 . For $\lambda < x^2$, the origin is a saddle point and the global minima are the two isolated rank-1 critical points⁴ cut out by the equations

$$w_2 w_1 = 1 - \lambda x^{-2}, \quad w_1 = w_2.$$

As λ increases toward x^2 , these minima move toward the origin, which remains a saddle point. As λ exceeds x^2 , the origin becomes the unique global minimum. This loss of information was our first hint at the connection to probabilistic PCA formalized in Theorem 3.1.

2.2. Denoising and contractive autoencoders

Two of the most well-studied regularized autoencoder models are the *denoising autoencoder* (DAE) and the *contractive autoencoder* (CAE) (Alain et al., 2012). In the linear case, their loss functions mirror the product and sum losses, respectively.

A linear DAE receives a corrupted data matrix \tilde{X} and is trained to reconstruct X by minimizing

$$\mathcal{L}_{\text{DAE}}(W_1, W_2) = \|X - W_2 W_1 \tilde{X}\|_F^2.$$

As shown in Pretorius et al. (2018), if $\tilde{X} = X + \epsilon$ is the corrupting process, where $\epsilon \in \mathbb{R}^{m \times n}$ is a noise matrix with elements sampled iid from a distribution with mean zero and variance s^2 , then

$$\mathbb{E}[\mathcal{L}_{\text{DAE}}] = \frac{1}{2n} \sum_{i=1}^n \|x_i - W_2 W_1 x_i\|^2 + \frac{s^2}{2} \text{tr}(W_2 W_1 W_1^\top W_2^\top).$$

With $\lambda = ns^2$, we have

$$\mathbb{E}[\mathcal{L}_{\text{DAE}}] = \frac{1}{2n} \mathcal{L}_\pi.$$

The loss function of a linear CAE includes a penalty on the derivative of the encoder:

$$\mathcal{L}_{\text{CAE}}(W_1, W_2) = \mathcal{L}(W_1, W_2) + \gamma \|J_f(x)\|_F^2.$$

³Identified with the components of $\text{GL}_1(\mathbb{R}) \cong \mathbb{R} \setminus \{0\}$.

⁴Identified with the components of $\text{O}_1(\mathbb{R}) \cong \{\pm 1\}$.

As shown in Rifai et al. (2011), if the encoder and decoder are tied by requiring $W_1 = W_2^\top$, then \mathcal{L}_{CAE} equals \mathcal{L}_σ with $\lambda = \frac{\gamma}{2}$:

$$\mathcal{L}_{\text{CAE}}(W_1) = \mathcal{L}_\sigma(W_1, W_1^\top).$$

In Theorem 2.1 we prove that the critical points of \mathcal{L}_{CAE} are identical to those of \mathcal{L}_σ even when the encoder and decoder are not tied.

2.3. Regularization and orthogonality

While \mathcal{L}_σ is not $\text{GL}_k(\mathbb{R})$ -invariant, it is still invariant under the length-preserving action of $\text{O}_k(\mathbb{R})$. In fact, L_2 -regularization reduces the symmetry group from $\text{GL}_k(\mathbb{R})$ to $\text{O}_k(\mathbb{R})$, making the left singular vectors of the encoder and right singular vectors of the decoder well-defined.

Two related facts about the relationship between regularization and orthogonality have guided our intuition throughout this work:

1. Orthogonal matrices are the determinant ± 1 matrices of minimal Frobenius norm (i.e., the columns have minimal squared length among those spanning a unit volume parallelepiped, forming a hypercube). This fact follows from the AM-GM inequality after casting the problem in terms of singular values:

$$\min_{\sigma_i} \sum \sigma_i^2 \quad \text{s.t.} \quad \prod \sigma_i^2 = 1$$

achieves its minimum iff $\sigma_i^2 = 1$ for all i .

2. For $k = m$, among pairs (W_1, W_2) minimizing \mathcal{L} , those which also minimize $\|W_1\|_F^2 + \|W_2\|_F^2$ are (W_1, W_1^\top) with W_1 orthogonal. This fact follows from noting that minimizing \mathcal{L} is equivalent to $W_2 = W_1^{-1}$, hence

$$\|W_1\|_F^2 + \|W_2\|_F^2 = \sum \sigma_i^2 + \sigma_i^{-2},$$

which is similarly minimized iff $\sigma_i^2 = 1$ for all i .

While it was not immediately clear to us that the solutions to (2) are also the minima of \mathcal{L}_σ , Theorem 4.2 shows this is indeed the case as $\lambda \rightarrow 0$. The core property differentiating the sum loss is the following, proven in the Appendix. In the following statement, $+$ denotes Moore–Penrose pseudoinverse).

Theorem 2.1 (Transpose Theorem). *While critical points of \mathcal{L} satisfy $W_1 = W_2^+$, those of \mathcal{L}_σ satisfy $W_1 = W_2^\top$.*

3. Bayesian Models

In this section, we identify Bayesian counterparts of our three loss functions and derive a novel connection between (regularized) LAEs and (probabilistic) PCA. This connection enables the application of any LAE training method to Bayesian MAP estimation of the corresponding model.

Consider the rank- k (self-)regression model

$$x_i = W_2 W_1 x_i + \varepsilon_i = W x_i + \varepsilon_i$$

where W_1 and W_2 act through their product W and $\varepsilon_i \sim \mathcal{N}_m(0, 1)$.

- \mathcal{L} is *rank- k regression*. The prior on W is the uniform distribution on $\mathbb{R}^{m \times m}$ restricted to rank- k matrices⁵.
- \mathcal{L}_π is *rank- k ridge regression*. The prior on W is $\mathcal{N}_{m \times m}(0, \lambda^{-1})$ restricted to rank- k matrices.
- \mathcal{L}_σ is the model with W_1 and W_2^\top independently drawn from $\mathcal{N}_{k \times m}(0, \lambda^{-1})$.

Theorem 4.2 shows that the minima of \mathcal{L}_σ , or equivalently the MAP of the Bayesian model, are such that W_2 is the orthogonal projection onto the top k principal directions followed by compression in direction i via multiplication by the factor $(1 - \lambda \sigma_i^{-2})^{\frac{1}{2}}$ for $\sigma_i^2 > \lambda$ and zero otherwise. Notably, for principal directions with eigenvalues dominated by λ , all information is lost no matter the number of data points. The same phenomenon occurs for pPCA with respect to eigenvalues dominated by the variance of the noise, σ^2 . Let's consider these Bayesian models side by side, with $W_0 \in \mathbb{R}^{m \times k}$ the parameter of pPCA⁶:

Bayesian \mathcal{L}_σ	pPCA
$W_1, W_2^\top \sim \mathcal{N}_{k \times m}(0, \lambda^{-1})$	$z_i \sim \mathcal{N}_k(0, 1)$
$\varepsilon_i \sim \mathcal{N}_m(0, 1)$	$\epsilon_i \sim \mathcal{N}_m(0, \sigma^2)$
$x_i = W_2 W_1 x_i + \varepsilon_i$	$x_i = W_0 z_i + \epsilon_i$

Comparing the critical points of \mathcal{L}_σ in Theorem 4.2,

$$W_1^\top = W_2 = U_{\mathcal{I}}(I_\ell - \lambda \Sigma_{\mathcal{I}}^{-2})^{\frac{1}{2}} O^\top, \quad (2)$$

and pPCA (Tipping & Bishop, 1999),

$$W_0 = U_{\mathcal{I}} \Sigma_{\mathcal{I}}(I_\ell - \sigma^2 \Sigma_{\mathcal{I}}^{-2})^{\frac{1}{2}} O^\top, \quad (3)$$

where $O \in \mathbb{R}^{k \times \ell}$ with orthonormal columns, we see that λ corresponds to σ^2 (rather than the precision σ^{-2}) in the sense that principal directions with eigenvalues dominated by either are collapsed to zero. The critical points only differ in the factor by which the remaining principal directions are shrunk. More precisely:

Theorem 3.1 (pPCA Theorem). *With $\sigma^2 = \lambda$, the critical points of*

$$\mathcal{L}_\sigma(W_0) = \mathcal{L}_\sigma(W_0^\top (X X^\top)^{-\frac{1}{2}}, (X X^\top)^{-\frac{1}{2}} W_0)$$

coincide with the critical points of pPCA.

⁵Note that rank- $(k-1)$ matrices are a measure zero subset of rank- k matrices.

⁶See Chapter 12.2 of Bishop (2006) for background on pPCA.

Proof. Multiplying the expression for W_2 in (2) on the left by $(X X^\top)^{\frac{1}{2}}$ gives the expression for W_0 in (3). \square

Interestingly, the generative model for \mathcal{L}_σ^0 is *not* that of pPCA. In the scalar case $n = m = k = 1$, $\mathcal{L}_\sigma^0(w_0)$ is

$$x^2 (1 - x^{-2} w_0^2)^2 + 2\lambda x^{-2} w_0^2$$

whereas the negative log likelihood of pPCA is

$$\frac{1}{2} (\ln(2\pi) + \ln(w_0^2 + \sigma^2) + x^2(w_0^2 + \sigma^2)^{-1}).$$

4. Loss Landscapes

Having contextualized LAE models in a Bayesian framework, we now turn to understanding their loss landscapes. Symmetries such as (1) exist because the model is expressed in an ‘‘overparameterized’’ coordinate form rooted in classical linear algebra and necessary for computer processing. This results in ‘‘flat’’ critical manifolds rather than a finite number of critical points. In Section 4.1, we remove all symmetries by expressing the loss geometrically over a topological domain. This results in $\binom{m}{k}$ critical points, and in particular a unique minimum. This intuition will pay off in Section 4.2, where we fully characterize all three LAE loss landscapes.

4.1. Points and planes

We now consider reconstruction loss over the domain of k -dimensional planes through the origin in \mathbb{R}^m . This space has the structure of a $k(m - k)$ -dimensional smooth, compact manifold called the Grassmannian of k -planes in \mathbb{R}^m and denoted $\text{Gr}_k(\mathbb{R}^m)$ (Hatcher, 2002). We'll focus on a few simple examples.

- $\text{Gr}_1(\mathbb{R}^2)$ is the space of lines through the origin in the plane, which may be smoothly parameterized by a counterclockwise angle of rotation of the x -axis modulo the half turn that maps a line to itself.
- $\text{Gr}_1(\mathbb{R}^3)$ is the space of lines through the origin in 3-space, also known as the real projective plane. We can visualize $\text{Gr}_1(\mathbb{R}^3)$ as the northern hemisphere of the 2-sphere with equator glued by the antipodal map.
- $\text{Gr}_2(\mathbb{R}^3)$ is identified with $\text{Gr}_1(\mathbb{R}^3)$ by mapping a plane to its 1-dimensional orthogonal complement.

A point cloud X in \mathbb{R}^m determines a smooth function

$$\mathcal{L}_X : \text{Gr}_k(\mathbb{R}^m) \rightarrow \mathbb{R}$$

whose value on a k -plane is the sum of square distances from the points to the plane. Figure 2 depicts \mathcal{L}_X as a height function for $\text{Gr}_1(\mathbb{R}^2)$ and $\text{Gr}_1(\mathbb{R}^3)$. Note that the min and max in (a) are the principal directions u_1 and u_2 , while the min, saddle, and max in (b) are the principal directions u_1 ,

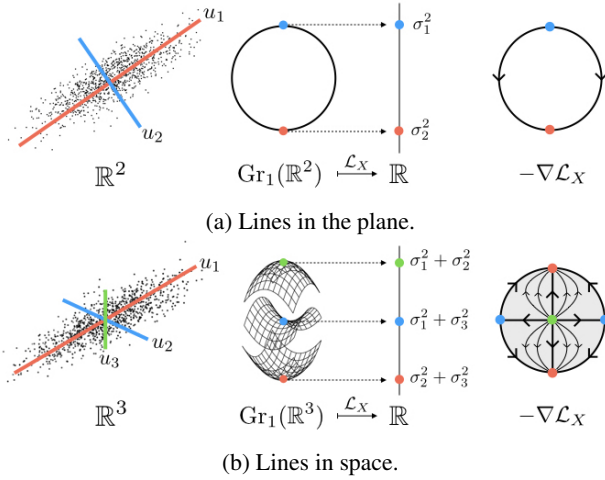


Figure 2. *Left*: Principal directions of a point cloud X . *Middle*: \mathcal{L}_X as height function on the manifold of lines through the origin. *Right*: Negative gradient flow of \mathcal{L}_X .

u_2 , and u_3 . At right, we depict the negative gradient flow $-\nabla \mathcal{L}_X$ on each space, with (b) represented as a disk with glued boundary. In (a), u_1 may descend to u_2 by rotating clockwise or counterclockwise⁷. In (b), u_1 may descend to u_2 or u_3 by rotating in either of two directions in the plane they span, and u_2 may similarly descend to u_3 .

The following theorem requires our assumption that the singular values of X are distinct. As a simple example, X could consist of one point on each coordinate axis:

$$\{(1, 0, \dots, 0), (0, 2, \dots, 0), \dots, (0, 0, \dots, m)\}.$$

Theorem 4.1 (Grassmannian Theorem). \mathcal{L}_X is a smooth function with $\binom{m}{k}$ critical points given by all rank- k principal subspaces. Near the critical point with principal directions $i_1 < \dots < i_k$, \mathcal{L}_X takes the form of a non-degenerate saddle with

$$d_{\mathcal{I}} = \sum_{j=1}^k i_j - j. \quad (4)$$

descending directions.

The latter formula counts the total number of pairs $i < j$ with $i \in \mathcal{I}$ and $j \notin \mathcal{I}$. These correspond to directions to flow along $-\nabla \mathcal{L}_X$ by rotating one principal direction u_i to another u_j of higher eigenvalue, fixing the rest.

In Appendix B, we prove a stronger form of the Grassmannian Theorem by combining Theorem 4.2, the commutative diagram 15 relating \mathcal{L}_X and \mathcal{L} , and techniques from algebraic topology.

⁷Formally, we mean there are two geometric gradient trajectories that converge to u_1 and u_2 in each time direction asymptotically, namely the left and right halves of the circle.

4.2. Coordinates

Translating the Grassmannian Theorem back to the coordinate representation $\mathbb{R}^{k \times m} \times \mathbb{R}^{m \times k}$ introduces two additional phenomena we saw in the scalar case in Section 2.1.

- Each critical point on $\text{Gr}_k(\mathbb{R}^m)$ corresponds to a manifold of rank- k critical points: $\text{GL}_k(\mathbb{R})$ or $\text{O}_k(\mathbb{R})$.
- Critical manifolds appear with rank less than k . In particular, $(0, 0)$ is a critical point for all three losses.

Now let's now combine our topological and scalar intuition to understand the the loss landscapes of LAEs in all dimensions and for all three losses.

Theorem 4.2 requires our assumption that X has distinct singular values $\sigma_1 > \dots > \sigma_m > 0$. Let u_1, \dots, u_m denote the corresponding left singular vectors (or principal directions) of X . For an index set $\mathcal{I} \subset \{1, \dots, m\}$ and $A \in \mathbb{R}^{m \times m}$ we define:

- $\ell = |\mathcal{I}|$ and increasing indices $i_1 < \dots < i_\ell$,
- $\Sigma_{\mathcal{I}} = \text{diag}(\sigma_{i_1}, \dots, \sigma_{i_\ell}) \in \mathbb{R}^{\ell \times \ell}$,
- $A_{\mathcal{I}} \in \mathbb{R}^{m \times \ell}$ consisting of columns i_1, \dots, i_ℓ of A .

Fix $\lambda > 0$. For the sum loss result, we also assume that λ is distinct from all σ_i^2 .

Theorem 4.2 (Landscape Theorem). As submanifolds of $\mathbb{R}^{k \times m} \times \mathbb{R}^{m \times k}$, the critical landscapes of \mathcal{L} and \mathcal{L}_π are smoothly parameterized by pairs (\mathcal{I}, G) , where $\mathcal{I} \subset \{1, \dots, m\}$ has size at most k and $G \in \mathbb{R}^{k \times \ell}$ has full rank; and with smooth structure that of the disjoint union of open submanifolds of $\mathbb{R}^{k \times \ell}$ given by ℓ -frames in \mathbb{R}^k .

As a submanifold of $\mathbb{R}^{k \times m} \times \mathbb{R}^{m \times k}$, the critical landscape of \mathcal{L}_σ is smoothly parameterized by pairs (\mathcal{I}, O) where $0 \leq \ell \leq \min\{k, m_0\}$ and m_0 is the largest index such that $\sigma_{m_0}^2 > \lambda$, $\mathcal{I} \subset \{1, \dots, m\}$ has size at most k , and $O \in \mathbb{R}^{k \times \ell}$ has orthonormal columns; and with smooth structure that of the disjoint union of Stiefel manifolds $V_\ell(\mathbb{R}^k)$ given by orthonormal ℓ -frames in \mathbb{R}^k .

These diffeomorphisms map (\mathcal{I}, G) or (\mathcal{I}, O) to (W_1, W_2) as follows:

	W_2	W_1
\mathcal{L}	$U_{\mathcal{I}} G^+$	$G U_{\mathcal{I}}^T$
\mathcal{L}_π	$U_{\mathcal{I}} (I_\ell + \lambda \Sigma_{\mathcal{I}}^{-2})^{-\frac{1}{2}} G^+$	$G (I_\ell + \lambda \Sigma_{\mathcal{I}}^{-2})^{-\frac{1}{2}} U_{\mathcal{I}}^T$
\mathcal{L}_σ	$U_{\mathcal{I}} (I_\ell - \lambda \Sigma_{\mathcal{I}}^{-2})^{\frac{1}{2}} O^\top$	$O (I_\ell - \lambda \Sigma_{\mathcal{I}}^{-2})^{\frac{1}{2}} U_{\mathcal{I}}^T$

Corollary 4.2.1. Near any point on the critical manifold indexed by \mathcal{I} , all three losses take the form of a degenerate saddle with $d_{\mathcal{I}} + (k - \ell)(m - \ell)$ descending directions.

- \mathcal{L} and \mathcal{L}_π have $k\ell$ flat directions.
- \mathcal{L}_σ has $k\ell - \binom{\ell+1}{2}$ flat directions.

Thus all three losses satisfy the strict saddle property⁸.

Proof. In addition to the descending directions of \mathcal{L}_X , there are $(k - \ell)(m - \ell)$ more that correspond to scaling one of $k - \ell$ remaining slots in G or O toward one of $m - \ell$ available principal directions⁹. The number of flat directions is given by the dimension of the symmetry group. For \mathcal{L} and \mathcal{L}_π , the ascending directions are the $k(m - k) - d_{\mathcal{I}}$ ascending directions of \mathcal{L}_X ; for \mathcal{L}_σ , an additional $\binom{\ell+1}{2}$ ascending directions preserve the reconstruction term while increasing the regularization term by decreasing orthogonality. \square

The proof of the Landscape Theorem 4.2 follows quickly from the Transpose Theorem 2.1 and Proposition 4.3 below.

Proposition 4.3. *Let $D, S \in \mathbb{R}^{m \times m}$ be diagonal matrices such that S is invertible and the diagonal of $D^2 S^{-2} D^2$ has distinct non-zero elements. Then the critical points of*

$$\mathcal{L}'(Q_1, Q_2) = \text{tr}(Q_2 Q_1 S^2 Q_1^\top Q_2^\top - 2Q_2 Q_1 D^2)$$

are smoothly parameterized by pairs (\mathcal{I}, G) where $\mathcal{I} \subset \{1, \dots, m\}$ has size at most k and $G \in \mathbb{R}^{k \times \ell}$ has full rank. The diffeomorphism is defined as follows:

	Q_2	Q_1
\mathcal{L}'	$D_{\mathcal{I}} S_{\mathcal{I}}^{-1} I_{\mathcal{I}} G^+$	$G I_{\mathcal{I}}^\top D_{\mathcal{I}} S_{\mathcal{I}}^{-1}$

Proof of Theorem 4.2. Given the singular value decomposition $X = U \Sigma V^\top$, let $Q_1 = W_1 U$ and $Q_2 = U^\top W_2$. By invariance of the Frobenius norm under the smooth action of the orthogonal group, we may instead parameterize the critical points of the following loss functions and then pull the result back to $W_1 = Q_1 U^\top$ and $W_2 = U Q_2$:

$$\begin{aligned} \mathcal{L}(Q_1, Q_2) &= \|\Sigma - Q_2 Q_1 \Sigma\|_F^2 \\ \mathcal{L}_\pi(Q_1, Q_2) &= \mathcal{L}(Q_1, Q_2) + \lambda \|Q_2 Q_1\|_F^2 \\ \mathcal{L}_\sigma(Q_1, Q_2) &= \mathcal{L}(Q_1, Q_2) + \lambda (\|Q_1\|_F^2 + \|Q_2\|_F^2) \end{aligned}$$

\mathcal{L} expands to

$$\text{tr}(Q_2 Q_1 \Sigma^2 Q_1^\top Q_2^\top - 2Q_2 Q_1 \Sigma^2 + \Sigma^2).$$

By Proposition 4.3 with $S = \Sigma$ and $D = \Sigma$, the critical points have the form

	Q_2	Q_1
\mathcal{L}	$I_{\mathcal{I}} G^+$	$G I_{\mathcal{I}}^\top$

⁸(Zhu et al., 2018). In the terminology of Appendix B, all three losses are *Morse-Bott functions*.

⁹In Figure 1c, these two gradient trajectories descend from the yellow saddle at 0 to the two red minima at $\pm u_1$.

\mathcal{L}_π expands to

$$\text{tr}(Q_2 Q_1 (\Sigma^2 + \lambda I) Q_1^\top Q_2^\top - 2Q_2 Q_1 \Sigma^2 + \Sigma^2).$$

By Proposition 4.3 with $S = (\Sigma^2 + \lambda I)^{\frac{1}{2}}$ and $D = \Sigma$, the critical points have the form

	Q_2	Q_1
\mathcal{L}_π	$I_{\mathcal{I}} (I_{\mathcal{I}} + \lambda \Sigma_{\mathcal{I}}^{-2})^{-\frac{1}{2}} G^+$	$G (I_{\mathcal{I}} + \lambda \Sigma_{\mathcal{I}}^{-2})^{-\frac{1}{2}} I_{\mathcal{I}}^\top$

By Lemma A.1 with $A = Q_2$ and $B = Q_1$, \mathcal{L}_σ expands to the sum of two functions:

$$\mathcal{L}_1(Q_1, Q_2) = \text{tr}(Q_2 Q_1 \Sigma^2 Q_1^\top Q_2^\top - 2Q_2 Q_1 (\Sigma^2 - \lambda I) + \Sigma^2)$$

$$\mathcal{L}_2(Q_1, Q_2) = \lambda \|Q_1 - Q_2^\top\|_F^2.$$

So at a critical point, $\nabla \mathcal{L}_1(Q_1, Q_2) = -\nabla \mathcal{L}_2(Q_1, Q_2)$ and $Q_1 = Q_2^\top$ by the Transpose Theorem 2.1. The latter also implies $\nabla \mathcal{L}_2(Q_1, Q_2) = 0$. So the critical points of \mathcal{L}_σ coincide with the critical points of \mathcal{L}_1 such that $Q_1 = Q_2^{\top 10}$.

By Proposition 4.3 with $S = \Sigma$ and $D = (\Sigma^2 - \lambda I)^{\frac{1}{2}}$, these critical points have the form

	Q_2	Q_1
\mathcal{L}_σ	$I_{\mathcal{I}} (I_{\mathcal{I}} - \lambda \Sigma_{\mathcal{I}}^{-2})^{\frac{1}{2}} O^\top$	$O (I_{\mathcal{I}} - \lambda \Sigma_{\mathcal{I}}^{-2})^{\frac{1}{2}} I_{\mathcal{I}}^\top$

In particular, real solutions do not exist for $\sigma_i^2 < \lambda$. \square

5. Empirical Illustration

In this section, we illustrate the Landscape Theorem 4.2 by training an LAE with synthetic and real data and visualizing properties of the learned weight matrices. All three losses satisfy the *strict saddle property* (Corollary 4.2.1), which implies that gradient descent and its extensions will reach a global minimum, regardless of the initialization, if trained for a sufficient number of epochs with a small enough learning rate (Zhu et al., 2018).

5.1. Synthetic data

In the following experiments, we set $k = \lambda = 10$ and fix a data set $X \in \mathbb{R}^{20 \times 20}$ with singular values $\sigma_i = i$ and random left and right singular vectors under Haar measure. We train the LAE for each loss using the Adam optimizer for 4000 epochs with random normal initialization and learning rate 0.05.

Figure 3 tracks the log squared distance between W_1 and W_2^\top during training. Indeed, only the the sum loss pulls the

¹⁰In fact, \mathcal{L}_σ has the same critical points if we add the constraint $W_2 = W_1^\top$ a priori as proven in Appendix A.

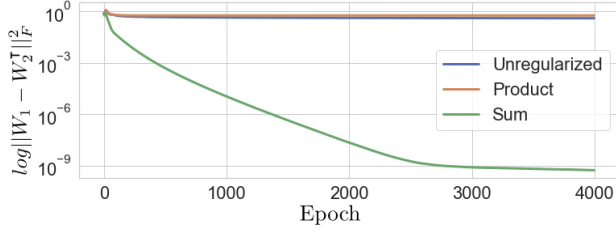


Figure 3. Distance between W_1 and W_2^T during training.

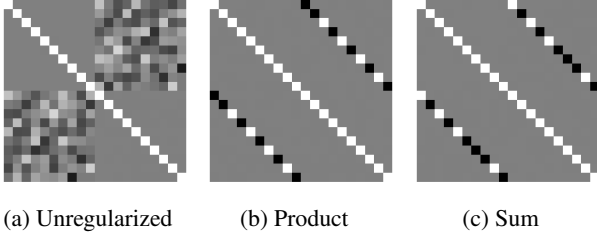


Figure 4. Heat map of the matrix $[U \ V_*]^T [U \ U_*]$. Black and white correspond to -1 and 1 , respectively.

encoder and (transposed) decoder together as claimed in the Transpose Theorem 2.1.

Let W_* be the product $W_2 W_1$ after training and fix the singular value decompositions

$$X = U \Sigma V^T, \quad W_* = U_* \Sigma_* V_*^T.$$

For each loss, the heat map of

$$\begin{bmatrix} U^T U & U^T U_* \\ V_*^T U & V_*^T U_* \end{bmatrix}$$

in Figure 4 is consistent with W_* approximating a global minimum defined by the Landscape Theorem. Namely, the lower right quadrant shows $U_* \approx V_*$ for each loss and the upper right and lower left quadrants show $U \approx U_*$ and $U \approx V_*$ up to column sign for the product and sum losses, *but not for the unregularized loss*. That is, for the product and sum losses, the left singular vectors of X are obtained as the right and left singular vectors of W_* .

The Landscape Theorem also gives explicit formulae for the eigenvalues of W_* at convergence. Letting σ_i^2 and τ_i^2 be the i^{th} largest eigenvalues of X and W_* , respectively, in Figure 5 we plot the points (σ_i^2, τ_i^2) for many values of λ . We superimpose a curve for each value of λ defined by the theoretical relationship between σ_i^2 and τ_i^2 in the Landscape Theorem. The (literal) alignment of theory and practice is visually perfect.

The Landscape Theorem also gives explicit forms for the encoder W_{1*} and decoder W_{2*} such that the matrices

$$A = \Sigma_*^{-\frac{1}{2}} U^T W_{2*} \quad \text{and} \quad B = W_{1*} U \Sigma_*^{-\frac{1}{2}} \quad (5)$$

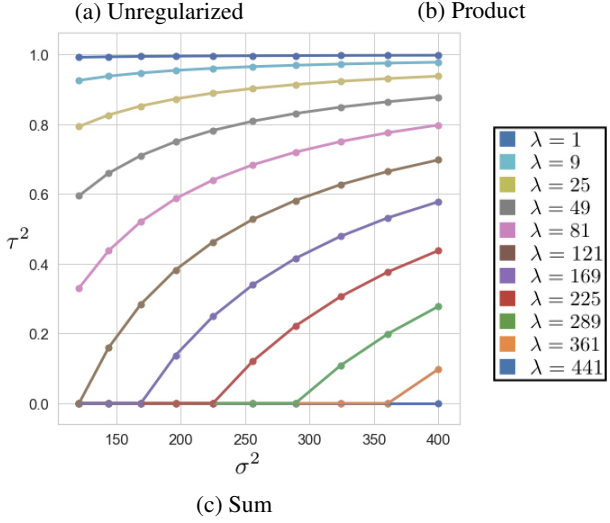
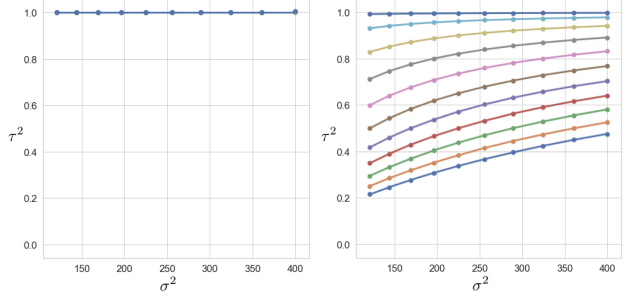


Figure 5. Illustration of the relationship between the eigenvalues of the weight matrix (τ^2) and data matrix (σ^2) for various values of λ . Points are the empirical and lines are theoretical.

satisfy $AB = I_k$ for all losses and are each orthogonal for the sum loss. In Figure 6, we illustrate these properties by applying the linear transformations A , B , and AB to the unit circle $\mathbb{S}^1 \subset \mathbb{R}^2$. Non-orthogonal transformations deform the circle to an ellipse, whereas orthogonal transformations (including the identity) preserve the unit circle.

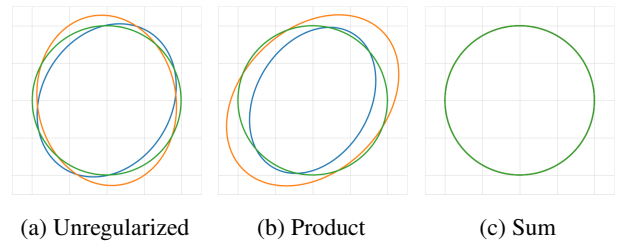


Figure 6. Image of the unit circle (green) under A (blue), B (orange), and AB (green) from (5). Non-orthogonal transformations deform the circle to an ellipse; orthogonal transformations preserve the circle.

5.2. MNIST

In the following experiment, the data set $X \in \mathbb{R}^{784 \times 10000}$ is the test set of the MNIST handwritten digit database (LeCun & Cortes). We train an LAE with $k = 9$ and $\lambda = 10$ for

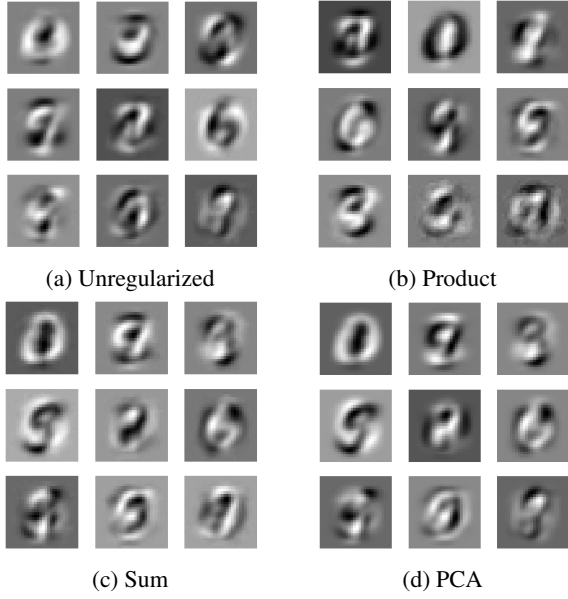


Figure 7. Left singular vectors of the decoder from an LAE trained on unregularized, product, and sum losses and the principal directions of MNIST reshaped into images.

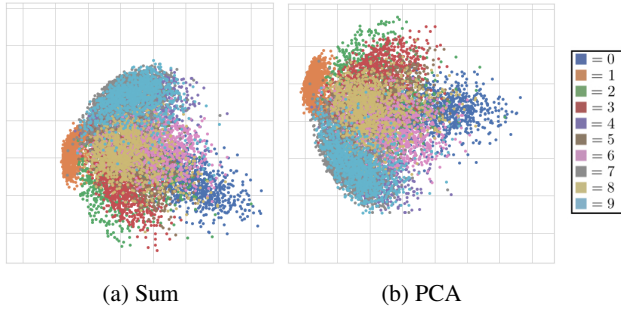


Figure 8. Latent representations of MNIST learned by an LAE with sum loss and by PCA. Colors represent class label.

each loss, again using the Adam optimizer for 100 epochs with random normal initialization, batch size of 32, and learning rate 0.05.

Figure 7 further illustrates the Landscape Theorem 4.2 by reshaping the left singular vectors of the trained decoder W_{2*} and the top k principal direction of X into 28×28 greyscale images. Indeed, only the decoder from the LAE trained on the sum loss has left singular vectors that match the principal directions up to sign.

As described in Section 3, for an LAE trained on the sum loss, the latent representation is, up to orthogonal transformation, the principal component embedding compressed along each principal direction. We illustrate this in Figure 8 by comparing the $k = 2$ representation to that of PCA.

6. Discussion

In 1989, Baldi & Hornik (1989) characterized the loss landscape of an LAE. In 2018, Zhou & Liang (2018) characterized the loss landscape of an autoencoder with ReLU activations on a single hidden layer. This paper fills out and ties together the rich space of research on linear networks over the last forty years by characterizing the loss landscapes of LAEs under several forms of regularization through a unified framework.

We proved and illustrated empirically that for LAEs trained under the standard (sum) form of L_2 regularization:

1. The encoder and decoder are transposes and well-defined up to orthogonal, as opposed to invertible, transformation in the latent space.
2. The critical points under the (reparameterized) sum loss are those of probabilistic PCA, even without tying the encoder and decoder as transposes *a priori*.
3. The principal directions exhibit a form of complete information loss more commonly associated with L_1 regularization.
4. For those eigenvalues greater than the regularization constant, both the singular values and left singular vectors of the data can be recovered through SVD of the encoder or decoder.

While the dataset X is $m \times n$ dimensional, the decoder is only $m \times k$ dimensional. This suggests *algorithmic experiments* to optimize scalable LAE training followed by SVD of the decoder as an efficient inference framework for (probabilistic) PCA and low-rank SVD. While many other methods have been proposed for recovering principal components with neural networks, they all require specialized algorithms for iteratively updating weights, similar to classical numerical SVD approaches (Warmuth & Kuzmin, 2007; Feng et al., 2013b;a). By contrast, training an L_2 -regularized LAE by SGD is more similar to modern randomized SVD methods, and has proven highly robust, scalable, and efficient with mini-batching in preliminary experiments.

This paper establishes a rigorous topological foundation for further exploration of the effects of regularization on loss landscapes. For example, in Appendix B we explain how this lens guarantees the empirical observation of valley passages between minima in Garipov et al. (2018). More recent ideas in algebraic topology¹¹ suggest applications of this view to other representation learning frameworks, such as non-negative matrix factorization, that may yield insights for improved training and robustness. By thinking deeply about how regularization encourages orthogonality in LAEs, this work also hints at new principles and algorithms for training deep nonlinear networks.

¹¹In particular, the extension of Morse homology to manifolds with boundary (Bloom, 2012)

A. Deferred Proofs

Proof of Theorem 2.1. Let $U\Sigma V^\top$ be the SVD of X , $Q_1 = W_1U$, and $Q_2 = U^\top W_2$. By orthogonal invariance of the Frobenius norm, $\mathcal{L}_\sigma(W_1, W_2)$ reduces to

$$\mathcal{L}_\sigma(Q_1, Q_2) = \|\Sigma - Q_2Q_1\Sigma\|_F^2 + \lambda(\|Q_1\|_F^2 + \|Q_2\|_F^2).$$

The critical landscape is defined by setting the partial derivatives to zero:

$$\frac{\partial \mathcal{L}_\sigma}{\partial Q_1} = 2Q_2^\top(Q_2Q_1 - I)\Sigma^2 + 2\lambda Q_1 = 0,$$

$$\frac{\partial \mathcal{L}_\sigma}{\partial Q_2} = 2(Q_2Q_1 - I)\Sigma^2 Q_1^\top + 2\lambda Q_2 = 0.$$

Multiplying the latter on the right by Q_2^\top gives

$$\Sigma^2(Q_2Q_1)^\top = (Q_2Q_1)\Sigma^2(Q_2Q_1)^\top + \lambda Q_2Q_2^\top \succeq 0,$$

which implies

$$\Sigma^2(Q_2Q_1)^\top \succeq (Q_2Q_1)\Sigma^2(Q_2Q_1)^\top.$$

Let $M = (Q_2Q_1 - I)\Sigma^2$. M is negative semi-definite by Lemma A.2 with $A = \Sigma^2$ and $B = Q_2Q_1$. Now note:

$$\frac{\partial \mathcal{L}_\sigma}{\partial Q_1} Q_1^\top = 0 \implies Q_2^\top M Q_1^\top = -\lambda Q_1 Q_1^\top \quad (6)$$

$$\frac{\partial \mathcal{L}_\sigma}{\partial Q_1} Q_2 = 0 \implies Q_2^\top M Q_2 = -\lambda Q_1 Q_2 \quad (7)$$

$$Q_1 \frac{\partial \mathcal{L}_\sigma}{\partial Q_2} = 0 \implies Q_1 M Q_1^\top = -\lambda Q_1 Q_2 \quad (8)$$

$$Q_2^\top \frac{\partial \mathcal{L}_\sigma}{\partial Q_2} = 0 \implies Q_2^\top M Q_1^\top = -\lambda Q_2^\top Q_2 \quad (9)$$

Since M and $Q_1 Q_1^\top$ are symmetric, (6) transposed gives:

$$Q_1 M Q_2 = -\lambda Q_1 Q_1^\top \quad (10)$$

Equality of (6) and (9) implies

$$Q_1 Q_1^\top = Q_2^\top Q_2,$$

while (7) or (8) each imply

$$Q_1 Q_2 \succeq 0.$$

Finally, (7) plus (9) minus (8) minus (10) gives

$$0 \succeq (Q_2^\top - Q_1)M(Q_2^\top - Q_1)^\top = 2\lambda(Q_1 Q_1^\top - Q_1 Q_2) \succeq 0.$$

The left-hand side is NSD since M is NSD. The right hand-side is PSD by Lemma A.3 with $A = Q_1$ and $B = Q_2^\top$. So both sides are zero, and in particular $Q_1 Q_1^\top = Q_1 Q_2$. Therefore

$$Q_1 Q_1^\top = Q_2^\top Q_2 = Q_1 Q_2,$$

which implies $Q_1 = Q_2^\top$ by Lemma A.4 with $A = Q_1$ and $B = Q_2^\top$. We conclude $W_1 = W_2^\top$. \square

Proof of Proposition 4.3. The critical landscape is defined by setting the partial derivatives to zero:

$$\frac{\partial \mathcal{L}'}{\partial Q_1} = 0 \implies Q_2^\top Q_2 Q_1 S^2 = Q_2^\top D^2 \quad (11)$$

$$\frac{\partial \mathcal{L}'}{\partial Q_2} = 0 \implies Q_2 Q_1 S^2 Q_1^\top = D^2 Q_1^\top \quad (12)$$

Let $Q = Q_2 Q_1$. Multiplying (11) on the right by D^{-2} and on the left by $D^{-2} S^2 Q_1^\top$ gives

$$D^{-2} S^2 Q^\top Q S^2 D^{-2} = D^{-2} S^2 Q^\top,$$

which implies $D^{-2} S^2 Q^\top$ is symmetric and idempotent. Multiplying (12) on the right by Q_2^\top gives

$$Q S^2 Q^\top = D^2 Q^\top,$$

which can be rewritten as

$$Q S^2 Q^\top = (D^2 S^{-2} D^2) (D^{-2} S^2 Q^\top).$$

Since the left-hand side is symmetric, $D^{-2} S^2 Q^\top$ is diagonal and idempotent by Lemma A.5 with $A = D^{-2} S^2 Q^\top$ and $B = D^2 S^{-2} D^2$. Lemma A.6 with the same A implies there exists an index set \mathcal{I} of size ℓ with $0 \leq \ell \leq k$ such that

$$D^{-2} S^2 Q^\top = I_{\mathcal{I}} I_{\mathcal{I}}^\top$$

and hence

$$Q = I_{\mathcal{I}} I_{\mathcal{I}}^\top D^2 S^{-2} = I_{\mathcal{I}} D_{\mathcal{I}}^2 S_{\mathcal{I}}^{-2} I_{\mathcal{I}}^\top. \quad (13)$$

Consider the smooth map $(Q_1, Q_2) \mapsto (\mathcal{I}, G)$ with

$$G = Q_1 S_{\mathcal{I}} D_{\mathcal{I}}^{-1} I_{\mathcal{I}}$$

from the critical submanifold of $\mathbb{R}^{k \times m} \times \mathbb{R}^{m \times k}$ to the manifold of pairs (\mathcal{I}, G) with G full-rank. Note

$$G^+ = I_{\mathcal{I}}^\top S_{\mathcal{I}} D_{\mathcal{I}}^{-1} Q_2$$

by (13). Commuting diagonal matrices to rearrange terms in (11) and (12), we obtain a smooth inverse map from pairs (\mathcal{I}, G) to critical points:

$$Q_1 = Q_1 S^2 Q^\top D^{-2} = Q_1 I_{\mathcal{I}} I_{\mathcal{I}}^\top = G I_{\mathcal{I}}^\top D_{\mathcal{I}} S_{\mathcal{I}}^{-1},$$

$$Q_2 = D^{-2} S^2 Q^\top Q_2 = I_{\mathcal{I}} I_{\mathcal{I}}^\top Q_2 = D_{\mathcal{I}} S_{\mathcal{I}}^{-1} I_{\mathcal{I}} G^+.$$

\square

Loss landscape with $W_2 = W_1^\top$ constraint. \mathcal{L}_σ has the same critical points if we add the constraint $W_2 = W_1^\top$ a priori:

$$\begin{aligned} \mathcal{L}_\sigma(W_1, W_1^\top) &= \|X - W_1^\top W_1 X\|_F^2 + 2\lambda \|W_1\|_F^2 \\ &= \|\Sigma - Q_1^\top Q_1 \Sigma\|_F^2 + 2\lambda \|Q_1\|_F^2 \\ &= \text{tr}(Q_1^\top Q_1 \Sigma^2 Q_1 - 2Q_1^\top Q_1 (\Sigma^2 - \lambda I) + \Sigma^2) \\ &= \mathcal{L}_1(Q_1, Q_1^\top). \end{aligned}$$

\square

Equating bias parameters and mean centering. Consider the loss function

$$\mathcal{L}_\beta(W_1, W_2, b_1, b_2) = \|X - W_2(W_1X + b_1e_n^\top) + b_2e_n^\top\|_F^2,$$

where $b_1 \in \mathbb{R}^k$ and $b_2 \in \mathbb{R}^m$ are bias vectors and $e_n \in \mathbb{R}^n$ is the vector of ones. With $b = W_2b_1 + b_2$, \mathcal{L}_b becomes

$$\|X - W_2W_1X - be_n^\top\|_F^2. \quad (14)$$

At a critical point,

$$\frac{\partial \mathcal{L}_\beta}{\partial b} = 2(X - W_2W_1X - be_n^\top)e_n = 0,$$

which implies

$$b = \frac{1}{n}Xe_n - W_2W_1\frac{1}{n}Xe_n.$$

Substituting into (14), \mathcal{L}_b reduces to

$$\|\bar{X} - W_2W_1\bar{X}\|_F^2$$

with $\bar{X} = X - \frac{1}{n}Xe_ne_n^\top$. Thus, at the optimal bias parameters, \mathcal{L}_β with X is equivalent to \mathcal{L} with X mean-centered. \square

Lemma A.1. Let $A \in \mathbb{R}^{m \times k}$ and $B \in \mathbb{R}^{k \times m}$, then

$$\|A\|_F^2 + \|B\|_F^2 = \|A - B^\top\|_F^2 + 2\text{tr}(AB)$$

Proof.

$$\begin{aligned} \|A - B^\top\|_F^2 &= \text{tr}((A - B^\top)^\top(A - B^\top)) \\ &= \text{tr}(A^\top A - A^\top B^\top - BA + B^\top B) \\ &= \|A\|_F^2 + \|B\|_F^2 - 2\text{tr}(AB) \end{aligned}$$

\square

Lemma A.2. Let $A, B \in \mathbb{R}^{m \times m}$. If $A \succeq 0$ and $AB^\top \succeq BAB^\top$, then $A \succeq BA$.

Proof. We express $A - BA$ as a sum of PSD terms:

$$A - BA = (B - I)A(B - I)^\top + (AB^\top - BAB^\top)$$

\square

Lemma A.3. Let $A, B \in \mathbb{R}^{m \times k}$. If $AA^\top = BB^\top$ and $AB^\top \succeq 0$, then $AA^\top \succeq AB^\top$.

Proof.

$$\begin{aligned} AA^\top - AB^\top &= \frac{1}{2}(AA^\top - AB^\top - BA^\top + BB^\top) \\ &= \frac{1}{2}(A - B)(A - B)^\top \succeq 0. \end{aligned}$$

\square

Lemma A.4. Let $A, B \in \mathbb{R}^{m \times k}$. If $AA^\top = BB^\top = AB^\top$ then $A = B$.

Proof. AA^\top is symmetric so $AB^\top = BA^\top$ and

$$(A - B)(A - B)^\top = AA^\top - AB^\top - BA^\top + BB^\top.$$

vanishes. We conclude $A - B = 0$. \square

Lemma A.5. Let $A, B \in \mathbb{R}^{m \times m}$ with B diagonal with distinct diagonal elements. If $AB = BA$ then A is diagonal.

Proof. Expand the difference of (i, j) elements:

$$\begin{aligned} (AB)_{ij} - (BA)_{ij} &= a_{ij}b_{jj} - b_{ii}a_{ij} \\ &= a_{ij}(b_{jj} - b_{ii}) = 0 \end{aligned}$$

So for $i \neq j$, $b_{ii} \neq b_{jj}$ implies $a_{ij} = 0$. \square

Lemma A.6. If $A \in \mathbb{R}^{m \times m}$ is diagonal and idempotent then $a_{ii} \in \{0, 1\}$.

Proof. $0 = (AA - A)_{ii} = a_{ii}^2 - a_{ii} = a_{ii}(a_{ii} - 1)$. \square

B. Morse homology of the real Grassmannian

This section embraces the language and techniques of differential and algebraic topology to dive into the topology underlying LAEs. To complement Wikipedia, the following resources cover the italicized terminology in depth: (Milnor, 1963; Hatcher, 2002; Banyaga & Hurtubise, 2004).

Let M be a smooth, compact manifold. In this section, we prove the Grassmannian Theorem through the lens of *Morse theory*, a subfield of differential and algebraic topology that relates the topology of M to smooth functions $f: M \rightarrow \mathbb{R}$.

A critical point of f is *non-degenerate* if the eigenvalues of the Hessian are non-zero. A *Morse function* is a smooth function all of whose critical points are non-degenerate. Morse functions are generic and stable; see Section 4.2 of Bloom (2004) for precise statements.

The *Morse index* d of a critical point is the number of negative eigenvalues of the Hessian. At each index- d non-degenerate critical point, one can choose a local coordinate system under which the function takes the form

$$-x_1^2 - \dots - x_d^2 + x_{d+1}^2 + \dots + x_m^2.$$

Hence $d = 0$ and $d = m$ correspond to parabolic minima and maxima, respectively, which all other values of d correspond to saddles with, in local coordinates, d orthogonal descending directions and $m - d$ orthogonal ascending directions. For example, the red, blue, and green critical points in Figure 2 have Morse indices 0, 1, and 2, respectively. \square

The *Morse inequalities* state that any Morse function on M must have at least as many index- d critical points as the *Betti number* b_d , i.e. the rank of the *singular homology group* $H_d(M; \mathbb{Z})$. This follows from a realization, called *Morse homology*, of singular homology as the homology of a chain complex generated in dimension d by the index- d critical points. The boundary map ∂ counts negative gradient trajectories between critical points of adjacent index. A Morse function is perfect if this signed count is always zero, in which case ∂ vanishes. A Morse function is \mathbb{F}_2 -perfect if this count is always even, in which case ∂ vanishes over the field of two elements.

Not all smooth manifolds admit perfect Morse functions. For example, the projective plane $\mathbb{RP}^2 \cong \text{Gr}_1(\mathbb{R}^3)$ cannot since $H_1(\mathbb{RP}^2; \mathbb{Z}) \cong \mathbb{F}_2$ implies that ∂ is non-zero. The *Poincaré homology sphere* is a famous example of a manifold without a perfect Morse over \mathbb{Z} or any field; this follows from *3-dimensional Poincaré conjecture*. The *smooth 4-dimensional Poincaré conjecture*, whose resolution continues to drive the field, states that there is only one smooth structure on the topological 4-sphere. This conjecture holds if and only if every smooth 4-sphere admits a perfect Morse function.

The Grassmannian $\text{Gr}_k(\mathbb{R}^m)$ provides a coordinate-free representation of the space of rank- k orthogonal projections, a submanifold of $\mathbb{R}^{m \times m}$. Through the identification of a projection with its image, $\text{Gr}_k(\mathbb{R}^m)$ is endowed with the structure of a smooth, compact Riemannian manifold of dimension $k(m - k)$.

Theorem B.1. \mathcal{L}_X is an \mathbb{F}_2 -perfect Morse function. Its critical points are the rank- k principal subspaces.

Proof. Consider the commutative diagram

$$\begin{array}{ccc} V_k(\mathbb{R}^m) & \xrightarrow{\pi: O \mapsto \text{Im}(OO^\top)} & \text{Gr}_k(\mathbb{R}^m) \\ \downarrow \iota: O \mapsto (O^\top, O) & & \downarrow \mathcal{L}_X \\ \mathbb{R}^{k \times m} \times \mathbb{R}^{m \times k} & \xrightarrow{\mathcal{L}} & \mathbb{R} \end{array} \quad (15)$$

where $V_k(\mathbb{R}^m)$ is the *Stiefel manifold* of $m \times k$ matrices with orthonormal columns. Since ι is an immersion, by Theorem 4.2 the critical points of $\mathcal{L} \circ \iota = \mathcal{L}_X \circ \pi$ are all k -frames spanning principal subspaces of X . Since π is a submersion, the critical points of \mathcal{L}_X are the image of this subset under π as claimed.

Each critical point (that is, rank- k principle subspace) is non-degenerate because each of the included k principal directions may be rotated toward any of the excluded $m - k$ principal directions in the plane they span, fixing all other principal directions; this accounts for all $k(m - k)$ dimensions. Flowing from higher to lower eigenvalues, these rotations are precisely the $-\nabla \mathcal{L}_X$ trajectories between adjacent

index critical points. Since there are exactly two directions in which to rotate, we conclude that \mathcal{L}_X is \mathbb{F}_2 -perfect. \square

While this paper may be the first to directly construct an \mathbb{F}_2 -perfect Morse function on the real Grassmannian, the existence of some \mathbb{F}_2 -perfect Morse function is straightforward to deduce from the extensive literature on perfect Morse functions on complex Grassmanians (Hansen, 2012; Duan, 2004). Our simple and intuitive function is akin to that recently established for the special orthogonal group (Solgun, 2016).

We encourage the reader to check the Morse index formula (4) in the case of $\text{Gr}_2(\mathbb{R}^4)$ in the table below. The symmetries of the table reflect the duality between a plane and its orthogonal complement in \mathbb{R}^4 .

d	i_1	i_2	i_3	i_4
0	•	•		
1	•		•	
2	•			•
2		•	•	
3		•		•
4			•	•

Theorem 2 implies that \mathcal{L}_X endows $\text{Gr}_k(\mathbb{R}^m)$ with the structure of a *CW complex*; each index- d critical point P is the maximum of a d -dimensional cell consisting of all points that asymptotically flow up to P . This decomposition coincides with the classical, minimal CW construction of Grassmannians in terms of *Schubert cells*. Over \mathbb{Z} , pairs of rotations have the same sign when flowing from even to odd dimension, and opposite signs when flowing from odd to even dimension, due to the oddness and evenness of the antipodal map on the boundary sphere, respectively. In this way, Morse homology for \mathcal{L}_X realizes the same chain complex as *CW homology*.

Morse homology also implies that if M is connected, i.e.,

$$b_0 = \text{rank } H_0(M; \mathbb{Z}) = 1,$$

then the bipartite graph of minima and index-1 saddles linked by gradient trajectories is connected as well¹². Hence, from the lens of algebraic topology, the empirical observation of such valley passages between modes in Garipov et al. (2018), which underlies their state-of-the-art Fast Geometric Ensembling training procedure, is *topologically inevitable*. And since \mathbb{R}^m is contractible, their method should in principle extend to finding all critical points of all indices, flowing along gradient trajectories from one minimum, to all minima and index-1 saddles, to all index-2 saddles, and so on.

¹²For example, in Figure 1(c), the red minima are each connected to the yellow saddle by one gradient trajectory, so the graph has three nodes and two edges connected in a path.

Acknowledgements

We thank Mehrtash Babadi, Matthew J. Johnson, Vardan Papyan, and Patrick Schultz for helpful discussions.

References

- Alain, G., Bengio, Y., and Rifai, S. Regularized autoencoders estimate local statistics. *CoRR*, abs/1211.4246, 2012.
- Baldi, P. and Hornik, K. Neural networks and principal component analysis: Learning from examples without local minima. *Neural Networks*, 2(1):53–58, 1989.
- Banyaga, A. and Hurtubise, D. *Lectures on Morse Homology*. Springer Netherlands, 2004.
- Bishop, C. M. *Pattern Recognition and Machine Learning*. Springer, 2006.
- Bloom, J. M. The local structure of smooth maps of manifolds, 4 2004. URL <http://www.math.harvard.edu/theses/phd/bloom/ThesisXFinal.pdf>.
- Bloom, J. M. The combinatorics of morse theory with boundary. *ArXiv e-prints*, 2012.
- Bourlard, H. and Kamp, Y. Auto-association by multilayer perceptrons and singular value decomposition. *Biological Cybernetics*, 59:291–294, 1988.
- Duan, H. Morse functions and cohomology of homogeneous spaces. 2004.
- Eckart, C. and Young, G. The approximation of one matrix by another of lower rank. *Psychometrika*, 1(3):211–218, 1936.
- Feng, J., Xu, H., Mannor, S., and Yan, S. Online pca for contaminated data. In *NIPS*, 2013a.
- Feng, J., Xu, H., and Yan, S. Online robust pca via stochastic optimization. In *NIPS*, 2013b.
- Garipov, T., Izmailov, P., Podoprikin, D., Vetrov, D., and Wilson, A. G. Loss surfaces, mode connectivity, and fast ensembling of dnns. In *NIPS*, 2018.
- Goodfellow, I., Bengio, Y., and Courville, A. *Deep Learning*. MIT Press, 2016. <http://www.deeplearningbook.org>.
- Hansen, M. C. Morse theory on complex grassmannians. Master’s thesis, University of Copenhagen, 6 2012.
- Hatcher, A. *Algebraic Topology*. Cambridge University Press, 2002.
- Izenman, A. Reduced-rank regression for the multivariate linear model. *Journal of Multivariate Analysis*, 5:248–264, 06 1975.
- Josse, J. and Wager, S. Bootstrap-based regularization for low-rank matrix estimation. *Journal of Machine Learning Research*, 17(124):1–29, 2016.
- LeCun, Y. and Cortes, C. <http://yann.lecun.com/exdb/mnist/>. URL <http://yann.lecun.com/exdb/mnist/>.
- Mehta, D., Chen, T., Tang, T., and Hauenstein, J. D. The loss surface of deep linear networks viewed through the algebraic geometry lens. *CoRR*, abs/1810.07716, 2018.
- Mianjy, P., Arora, R., and Vidal, R. On the implicit bias of dropout. In *ICML*, 2018.
- Milnor, J. *Morse Theory*. Princeton University Press, 1963.
- Mukherjee, A. and Zhu, J. Reduced rank ridge regression and its kernel extensions. *Statistical Analysis and Data Mining*, 4(6):612–622, 2011.
- Plaut, E. From principal subspaces to principal components with linear autoencoders. *ArXiv e-prints*, 2018.
- Pretorius, A., Kroon, S., and Kamper, H. Learning dynamics of linear denoising autoencoders. In *ICML*, 2018.
- Rifai, S., Vincent, P., Muller, X., Glorot, X., and Bengio, Y. Contractive auto-encoders: Explicit invariance during feature extraction. In *ICML*, 2011.
- Solgun, M. Perfect morse function on $SO(n)$. *European Journal of Pure and Applied Mathematics*, 9(3):314–321, 2016.
- Tipping, M. E. and Bishop, C. M. Probabilistic principal component analysis. *Journal of the Royal Statistical Society*, 61(3):611–622, 1999.
- Warmuth, M. K. and Kuzmin, D. Randomized online pca algorithms with regret bounds that are logarithmic in the dimension. 2007.
- Zhou, Y. and Liang, Y. Critical points of linear neural networks: Analytical forms and landscape properties. In *ICLR*, 2018.
- Zhu, Z., Li, Q., Tang, G., and Wakin, M. B. Global optimality in low-rank matrix optimization. *IEEE Transactions on Signal Processing*, 66(13):3614–3628, 2018.